Tridiagonal Fermi resonance structure in the IR spectrum of the excited CH chromophore in CF_3H

Hans-Rolf Dübal and Martin Quack
Laboratorium für Physikalische Chemie der ETH, ETH-Zentrum, CH-8092 Zürich, Switzerland

(Received 26 March 1984; accepted 22 June 1984)

The absorption spectrum of trifluoromethane has been recorded between 900 and 14 000 cm^{-1} with resolutions between 0.004 and 0.5 cm^{-1} (pressure broadened). 22 bands were assigned as arising from the interacting CH stretching and bending manifolds, which account for most of the absorption in the overtone region. The results can be understood quantitatively with an effective, tridiagonal many-level Fermi resonance Hamiltonian. The experimental and theoretical results are summarized in Table II. The Hamiltonian is given in Table III and shows a very large stretching–bending interaction constant $|k_{sbb}| = 106$ cm^{-1}, which is even larger than the diagonal anharmonic constant for the stretching vibration $|x'_{ss}| = 62$ cm^{-1}. This leads to extensive vibrational redistribution between stretching and bending motions at high levels of excitation. The time dependent redistribution is calculated with the spectroscopic Hamiltonian. A rotational analysis is presented for some of the bands involved in the Fermi resonance. The effect of the Fermi resonance on hot bands is investigated using the same Hamiltonian in comparison with experiment. The results are discussed in relation to the universal local dynamics of the isolated alkyl CH-stretching chromophore and in relation to the vibrational dynamics of highly excited polyatomic molecules as a function of certain elements of molecular structure.

I. INTRODUCTION

Intramolecular vibrational coupling in polyatomic molecules and the time dependent flow of energy between the rovibrational degrees of freedom is among the central questions in spectroscopy and unimolecular reaction dynamics.[1–4] This problem has been addressed recently using a variety of experimental[5–8] and theoretical[9–12] techniques. The main questions are: (i) To what extent can the IR fundamental and overtone absorptions be interpreted by localized initial excitations (local mode[13] or chromophore[14] states)? (ii) On which time scale and under which conditions is there intramolecular rovibrational redistribution corresponding spectroscopically to "global"[15] vibrational eigenstates? (iii) Can one identify relationships between structural elements in molecules and the corresponding vibrational dynamics? This implies the possible aim of tailoring molecules suitable for either statistical or mode selective chemistry.

One obvious experimental approach to answer these questions is the study of the high resolution rovibrational spectra of polyatomic molecules in order to obtain from this the rovibronic Hamiltonian and the related intramolecular dynamics. In spite of a large body of spectroscopic data, the number of systematic investigations with the specific aims mentioned above seems to be rather limited (see Refs. 1–5 for reviews). We have therefore initiated, some time ago,[14] a systematic study of the spectra and dynamics of the isolated CH chromophore. We give in the present paper the first detailed account of our results on an extensive redistribution occurring in the form of a tridiagonal Fermi resonance system in CF_3H. It turns out that this redistribution is a universal phenomenon of the isolated alkyl CH chromophore and some preliminary results have already been presented[16] with details on $(CF_3)_3CH$,[17] CD_3H,[18] and further systems[19] being reported separately.

CF_3H is an ideal model system for demonstrating the general features of this tridiagonal Fermi coupling and redistribution. It is a highly volatile substance of good isotopic purity. The CH transitions are particularly intense[14] and have a well defined polarization in this symmetric top molecule. Due to the mass ratios the local and normal mode motions coincide approximately. There is considerable spectroscopic ground work available.[20–32] One should mention in particular the high resolution studies of the fundamentals ν_6(508 cm^{-1}, E) and ν_3(700 cm^{-1}, A_1)[20] and of ν_4(ν_b hereafter, 1378 cm^{-1}, E),[21] the recent work on the coupled CF_3-stretching fundamentals $\nu_2(A_1)$ and $\nu_5(E)$,[22] and finally the strongly perturbed fundamental ν_1(ν_s hereafter, 3035 cm^{-1}, A_1).[23] Much of the early work under moderate resolution can be found discussed in the paper by Ruoff *et al.*[25] and there are a number of further relevant papers[26–28] also concerning the molecular constants for the vibrational ground state[29,30] and excited states.[31,32] Furthermore, CF_3H has been investigated recently for vibrational energy transfer in collisions with protons.[33]

Most important for our present work was in fact the early paper by Bernstein and Herzberg on the overtone spectra in the photographic infrared and visible regions.[24] These authors have already discovered some bands exhibiting a resonance between the stretching overtones $|v_s\rangle$ and the stretch–bend combinations $|v_s - 1, v_b = 2\rangle$, which was then interpreted as a classic two-level Fermi resonance.[34] In order to obtain a more complete understanding in terms of many-level interactions and the global, dominant coupling of the CH-stretching and bending vibrations we have measured the complete spectrum of CF_3H between the mid-IR, starting at 900 cm^{-1}, and the red part of the visible spectrum at 14 000 cm^{-1}, with resolutions corresponding to bandwidths (FWHM) between 0.004 cm^{-1} (apodized) and 0.5 cm^{-1} (pressure broadened). It turns out that almost all of the major bands in the overtone region can be understood on the

 0021-9606/84/213779-13$02.10

basis of a rather simple, effective Hamiltonian which provides us with a considerable insight into the nature of the coupling of the CH-stretching and bending vibrations.

II. EXPERIMENTAL

All spectra have been recorded on our BOMEM DA.002 interferometric Fourier transform spectrometer system. The Michelson interferometer has a maximum mirror displacement of 1.25 m and correspondingly an instrument function with an apodized lowest bandwidth (FWHM) of 0.004 cm^{-1} (best unapodized resolution 0.0024 cm^{-1}, resolving power $R = \tilde{\nu}/\delta\tilde{\nu} > 10^6$). For the IR work a mercury cadmium telluride detector and an indium antimonide detector were used in conjunction with KBr and CaF_2 beam splitters. For the near IR and visible spectral regions a quartz beam splitter was used together with a Si detector. The signal to noise ratios were greatly improved by the use of narrow band interference filters. A globar and a bright Philips lamp were used as light sources. Fundamentals and some overtone transitions were measured with single pass cells of lengths between 0.1 and 0.17 m. These were also used for absolute band strength measurements. In order to reduce the pressure broadening, most overtone spectra were taken with a multipass cell using White optics,[35] which allows for variable optical path lengths up to about 20 m. The effective optical path length of this cell was calibrated for intensity measurements by means of the integrated band strength of the overtone of $(CF_3)_3CH$ at 5880 cm^{-1}, whose absolute intensity has been measured previously.[14] Where the necessary calibrations were not possible, only relative intensity values are reported. In all intensity measurements the ratio of the pressure broadening width to the experimental bandwidth of the spectrometer was sufficiently large ($\geqslant 5$) that direct integration of the spectra was possible. The frequency calibration was obtained by reference to the wavelength of a single-mode He–Ne laser used for measuring interferometrically the relative optical displacement of the fixed and moving mirrors of the Michelson interferometer. Minor misalignments of the IR light with respect to the He–Ne laser beam generally may lead to small frequency errors of the order of the bandwidth of the measurement. Where possible, more accurate calibration was therefore obtained by means of the wave number tables in Ref. 36 and with CO, water, and methane lines in the overtone region.[37–39] The narrow absorption lines from the calibration measurements have also been used to check for the actual experimental bandwidth of the instrument function, which often depends upon the aperture and alignment conditions, due to self-apodization (minimum apertures of 0.5 mm diameter were used in our measurements).

$^{12}CF_3H$ was obtained from Merck–Darmstadt. Its identity was obvious from the spectra and neither the gas chromatogram nor the IR spectra showed substantial impurities apart from the natural ^{13}C isotope content. Where necessary the absence of air was ensured by degassing in several freeze–pump–thaw cycles before use. Some water is always present in the long path absorption measurements. This accounts for a negligible fraction of the integrated absorption and partial pressure for our conditions, although the narrow lines are often pronounced and easily visible. No attempt at excessive drying has been made because these lines are helpful for calibration purposes.

III. RESULTS AND DISCUSSION

A. Survey of multiple Fermi resonances

Figure 1 shows a survey transmission spectrum between 4000 and 9000 cm^{-1} for 5×10^4 Pa of CF_3H and an optical path of 22.5 m. Under these conditions, one easily recognizes three groups of strong transitions, one below 6000 cm^{-1}, corresponding to the first overtone CH-stretching system, one around 7000 cm^{-1}, corresponding to a combination of this with one quantum of the CH bending, and one between about 8000 and 9000 cm^{-1}, originating from the second overtone of the CH-stretching vibration. The two bands at 8792 and 8589 cm^{-1} have already been discussed by Bernstein and Herzberg as the Fermi dyad arising from the resonance between $|v_s = 3, v_b = 0\rangle$ and $|v_s = 2, v_b = 2\rangle$. However, under the conditions used for the spectrum in Fig. 1, two further bands are clearly visible, one at 8286 cm^{-1} and a very weak one with a line like Q branch at 7890 cm^{-1}. As we shall see below, these arise from complementing the simple Fermi dyad with the further interacting states $|v_s = 1, v_b = 4\rangle$ and $|v_s = 0, v_b = 6\rangle$. This results in a four-level Fermi polyad extending over a frequency range of 1000 cm^{-1} in this case. The band systems around 7000 cm^{-1} and below 6000 cm^{-1} find a similarly simple interpretation by

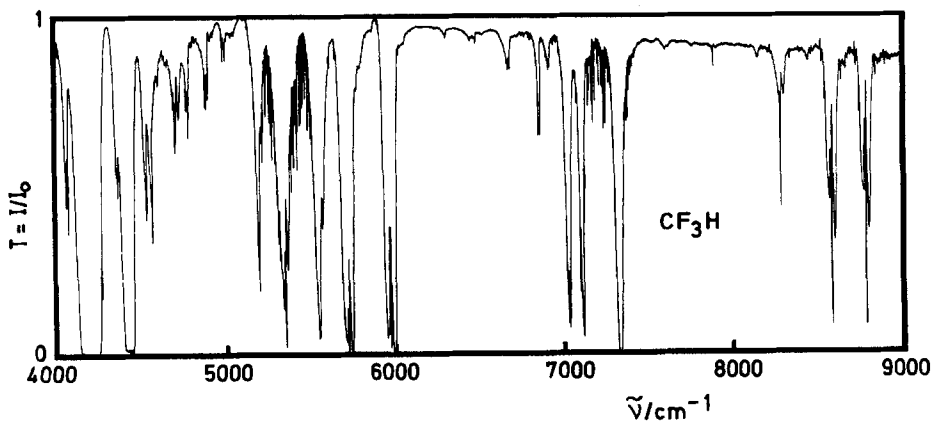

FIG. 1. The vapor phase transmission spectrum of CF_3H, survey between 4000 and 9000 cm^{-1}. ($P = 0.5 \times 10^5$ Pa, $l = 22.5$ m, resolution 1 cm^{-1}, the base line is not quite flat over such a large spectral range.)

means of Fermi polyads of the strongly interacting CH-stretching and bending vibrational modes.

B. Effective Hamiltonian for the tridiagonal Fermi resonance systems

In order to provide a rational, quantitative description of our experimental observations we define the diagonal elements of an effective spectroscopic Hamiltonian by means of the usual low order term formula,[1] which can be derived by perturbation theory[40–42]:

$$T_n = \sum_j \tilde{\nu}_j v_j + \sum_i \sum_{j>i} x_{ij} v_i v_j + \sum_i \sum_{j\geq i} g_{ij} l_i l_j. \tag{1}$$

We restrict our attention to the stretching (s) and bending (b) vibrations of CH and define a chromophore quantum number:

$$N = v_s + \tfrac{1}{2} v_b. \tag{2}$$

For the isolated alkyl CH vibrations the $N+1$ (or 1/2) states with a common N are members of a polyad and have about the same energy to within some bandwidth. They correspond to one chromophore "level." The diagonal matrix elements are given in cm^{-1} units:

$$H^N_{nn} = \tilde{\nu}'_s v_s + \tilde{\nu}'_b v_b + x'_{ss} v_s^2 + x'_{bb} v_b^2 + x'_{sb} v_s v_b + g'_{bb} l_b^2. \tag{3}$$

The quantum number l_b gives the vibrational angular momentum for the degenerate two-dimensional, approximately isotropic bending oscillator. In our spectra two values of l_b are important. For $l_b = 0$ we have polyads with $N+1$ states of A_1 vibronic symmetry in C_{3v} (2N = even):

$$|v_s, v_b, l_b = 0\rangle : \{|N, 0, 0\rangle, |N-1, 2, 0\rangle, \ldots, |0, 2N, 0\rangle\}. \tag{4}$$

For $l_b = 1$ we have polyads with $N + \frac{1}{2}$ states of E vibronic symmetry in C_{3v} ($2N$ = odd):

$$|v_s, v_b, l_b = 1\rangle : \{|N-1/2, 1, 1\rangle, |N-3/2, 3, 1\rangle, \ldots, |0, 2N, 1\rangle\}. \tag{5}$$

The vibrational Hamiltonian is assumed to be diagonal in l_b and block diagonal in N. Each block for a given N is a tridiagonal, symmetric matrix with off-diagonal elements:

$$H^N_{v_s v_b l_b, v'_s v'_b l'_b} = \langle v_s, v_b, l_b | k_{sbb} q_s q_b^2 | v'_s, v'_b, l'_b \rangle. \tag{6}$$

In the normal mode approximation the q are dimensionless reduced normal coordinates,[40] with the relationship for the bending vibration (two degrees of freedom 1 and 2):

$$q_b^2 = q_{b1}^2 + q_{b2}^2. \tag{7}$$

k_{sbb} is the corresponding effective cubic potential constant in cm^{-1} for the term $q_s q_b^2$ in the Taylor expansion of the potential function, including the 1/3! factor. The selection rules for the matrix elements in Eq. (6) are:

$$k_{sbb} \neq 0, \tag{8a}$$

$$v'_s = v_s \pm 1, \tag{8b}$$

$$v'_b = v_b \text{ or } v_b \pm 2, \tag{8c}$$

$$l'_b = l_b. \tag{8d}$$

The assumption of the block-diagonal structure allows us to define the resonance part of the coupling matrix:

$$H^N_{v_s v_b l_b, (v_s-1), (v_b+2), l_b} = \langle v_s, v_b, l_b | k_{sbb} q_s q_b^2 | v_s - 1, v_b + 2, l_b \rangle$$

$$= -\tfrac{1}{2} k_{sbb} \cdot [\tfrac{1}{2} v_s (v_b - l_b + 2)(v_b + l_b + 2)]^{1/2}. \tag{9}$$

In these equations we have made use of Eq. (7) and of the harmonic oscillator matrix elements in Ref. 41. Diagonalizing each block $\mathbf{H}^N$ of $\mathbf{H}$ one obtains the eigenvalues E_j^N and the eigenvector matrix $\mathbf{Z}_N$,[47]

$$\mathbf{Z}_N^T \mathbf{H}^N \mathbf{Z}_N = \mathrm{Diag}(E_1^N \cdots E_n^N). \tag{10}$$

When there is strong mixing even an approximate assignment of states by the v_s and v_b quantum numbers is impossible and we label the states by the symbol $(N)_j$, standing for the jth eigenstate of the Nth block. The quantum number j orders the eigenvalues in descending order (the notation is similar to the J_τ notation for asymmetric top rotational eigenvalues; however, N is a good quantum number only in the framework of our approximations, not exactly).

The absolute squares of the electric dipole transition moments satisfy the relationships

$$M^0_{v_s v_b l_b, 000}(\alpha) = \langle v_s, v_b, l_b | \hat{\mu}_\alpha | 0, 0, 0 \rangle, \tag{11}$$

$$M_{j0}(\alpha)_N = \langle N_j | \hat{\mu}_\alpha | 0, 0, 0 \rangle, \tag{12}$$

$$\sum_{j(N)} |M^0_{j0}(\alpha)|^2 = \sum_{j(N)} |M_{j0}(\alpha)_N|^2. \tag{13}$$

The sums are extended over all the states of one polyad and $\hat{\mu}_\alpha = \hat{\mu}_{x,y,z}$ is one component of the electric dipole operator $\hat{\mu}$. If only one zero order state, namely $|v_s, v_b = 0, l_b = 0\rangle$ or $|v_s, v_b = 1, l_b = 1\rangle$ has a nonvanishing $|M^0_{j0}|^2$ one can calculate the relative intensity for one polyad transition by means of the simplified equation (14):

$$g_j = |Z_{1j}|^2, \tag{14a}$$

$$\sum_j g_j = \sum_j |Z_{1j}|^2 = 1. \tag{14b}$$

This approximation is quite good for the overtone transitions, better for the A_1 polyads than for the E polyads. We shall compare the theoretical model results with experimental relative intensities defined by Eq. (15):

$$g_j^{\text{expt}} = G_j / \sum_{\text{polyad}} G_k. \tag{15}$$

The experimental G value is obtained from the high resolution absorptions cross section $\sigma(\tilde{\nu})$ by means of Eq. (16):

$$G_j = \int_{\text{band } j} \sigma(\tilde{\nu}) \left(\frac{d\tilde{\nu}}{\tilde{\nu}}\right) \simeq \frac{1}{\tilde{\nu}_0 c l} \int_{\text{band } j} \ln (I_0/I) d\tilde{\nu}, \tag{16}$$

$\tilde{\nu}_0$ is the band center, c the concentration of the absorber, l the absorption path, and I_0 and I the incident and transmitted intensities. G is related to the vibrational transition moment for nondegenerate bands by Eq. (17) (cgs system):

$$G_j = \frac{8\pi^3}{3hc} |M_{j0}|^2. \tag{17}$$

The effective spectroscopic Hamiltonian defined above is consistent with the approximate treatment of Nielsen.[43] We have suppressed on purpose all higher order corrections both in the diagonal elements [Eq. (3)] and the off-diagonal elements,[44] in order to minimize the number of parameters

to be determined experimentally (seven in the present model). As we shall see below, the Hamiltonian describes the experimental data very well (22 band positions *and* intensities), as we have also found for other molecules. A few words may be useful concerning the approximations involved. Equation (1) is derived in a standard way[40] in the normal mode approximation, with separable kinetic energy and retaining anharmonic corrections by low order perturbation theory. The diagonal elements in Eq. (3) contain the primed constants $\tilde{\nu}'$ and x' because we choose in this model to retain terms arising from k_{sbb} through resonance interaction explicitly by diagonalization. We have found for the analogous acetylene compounds, where the resonance does not occur, that the higher order terms beyond Eqs. (1) and (3) are measurable, but small, indeed, of the order of the deviations we obtain below when comparing experiment and theory. To the extent that the harmonic normal mode basis states are good representations of the states giving the term formula [Eq. (1)] the off-diagonal elements find a simple interpretation by means of the anharmonic potential constant k_{sbb}, again neglecting contributions from other terms in the potential. It is clear, however, that even for the diagonal part of **H** the deviations from harmonic basis states may become important. Furthermore, a curvilinear description for the large amplitude bending motion may be more appropriate, giving a reinterpretation of $\hat{H}_c = k_{sbb} q_s q_b^2$ in terms of both kinetic and potential energy coupling. This point has been discussed by Sibert, Hynes, and Reinhardt.[45] On the level of approximation used here this does *not* change the form of **H**. Because of our use of dimensionless q one has only to change the definition of k_{sbb} in Eq. (9).

The effective Hamiltonian can be interpreted in yet another way, which provides physical insight. Following our discussion of the CH-overtone spectra in substituted acetylenes R–C≡CH,[46] where the Fermi resonance does not occur, we can derive the diagonal part of the Hamiltonian matrix from a vibrationally adiabatic $\hat{H}_0$ with

$$\hat{H}_0 \psi^0_{nm} = E^0_{nm} \psi^0_{nm}, \tag{18}$$

$$\psi^0_{nm} = \phi_n(b, s) \xi_{nm}(b). \tag{19}$$

The ϕ_n are solutions of the "clamped b" Schrödinger equation (neglecting the bending kinetic energy):

$$\hat{H}(b, s) \phi_n(b, s) = V_n(b) \phi_n(b, s). \tag{20}$$

The $V_n(b)$ are the effective potentials for the bending coordinate for each quantum number $n = v_s$ of the "high frequency" stretching vibration. The adiabatic solution for both coordinates is given by Eq. (21), reintroducing now the kinetic energy $\hat{T}_b$ in the bending vibration

$$\{\hat{T}_b + \hat{V}_n(b)\} \xi_{nm}(b) = E^0_{nm} \xi_{nm}(b). \tag{21}$$

This solution gives the *diagonal* part of the Hamiltonian and is an immediate justification why in Eq. (3) the term $x'_{sb} v_s v_b$ appears, which is nondiagonal in the quantum numbers v_s and v_b: The quantity $(\tilde{\nu}_b + x'_{sb} v_s)$ is the bending frequency for the effective potential V_n with stretching quantum number $n = v_s$. This term would not appear if a completely separable basis were chosen for the diagonal part of **H**. In the vibrationally adiabatic approximation the off-diagonal coupling in Eq. (9) arises from the neglect of the kinetic energy in the bending vibration [Eqs. (18)–(20)]. It is clear that, quantitatively, the vibrationally adiabatic approximation for two degrees of freedom with just a factor of 2 difference in the characteristic frequency is poor and will break down completely as demonstrated by the resonance structure in the observed spectra. Of course, subsequent diagonalization of **H** remedies this deficiency of the approximation.

An approximation which remains, even after the diagonalization of the resonance blocks, is the neglect of the interpolyad coupling of different blocks, which is possible by means of allowed vibrational matrix elements, if the blocks have the same vibronic symmetry. The energy separation of the blocks is, however, more than a factor of five to ten larger than the coupling matrix elements, which makes the approximation practically useful although not quantitatively perfect. Finally, local rovibrational and vibrational resonances and perturbations due to the interactions with other modes have been neglected in the model Hamiltonian. We have seen such perturbations in numerous places in the spectra but they are much smaller than the effects considered here and can be neglected on the relevant time and energy scales.

C. The $N = 3$ resonance polyad

In order to illustrate the discussion in Sec. III B we present here the detailed results for the $N = 3$-A_1-polyad, which is the highest one for which *all* expected bands have been accessible to observation, so far. The basis states are

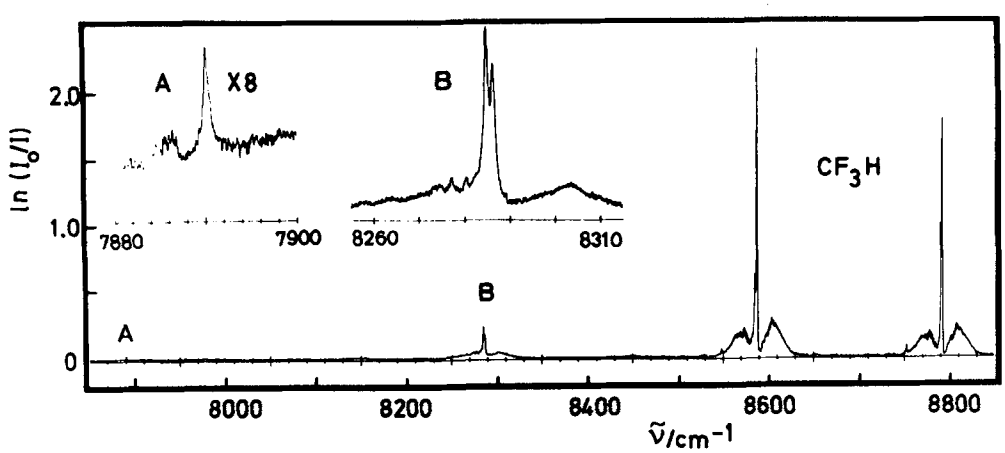

FIG. 2. Survey spectrum of the $N = 3$ Fermi resonance polyad in CF_3H. The inserts are magnified portions from the same survey spectrum ($P = 0.5 \times 10^5$ Pa, resolution 1 cm^{-1}.)

TABLE I. Comparison of the tridiagonal Fermi resonance model with experiment for the $N = 3$ polyad of fluoroform.

	Model		Experiment	
j	$\tilde{\nu}_j/\text{cm}^{-1}$	g_j	$\tilde{\nu}_j/\text{cm}^{-1}$	$g_j^{\text{expt.}}$
1	8792.20	0.529	8792.70	0.52
2	8589.28	0.431	8589.28	0.45
3	8285.53	0.039	8286.0	0.03
4	7887.75	0.001	7890	<0.01

$|3,0,0\rangle$, $|2,2,0\rangle$, $|1,4,0\rangle$, and $|0,6,0\rangle$. Figure 2 shows the four parallel bands of very different intensity, which are expected for the given frequency range. The assignment can be established without doubt due to the rotational structure and the agreement between the observed and calculated band positions and intensities, which are shown in Table I. The Hamiltonian was not adjusted to these few bands but is the one from the global fit given in the next section. Its structure is illustrated in Fig. 3. From the matrix elements in cm^{-1} shown in Fig. 3(b) one can see that the coupling matrix elements are large, of the order of the zero order energy differences. This leads to very extensive mixing and vibrational redistribution between all four states. On the other hand, the matrix elements are substantially smaller than the separation from the other polyads. This allows us to neglect the interpolyad coupling at least at this level of excitation (the approximation gets worse, the higher the energy).

D. Analysis of the vibrational spectrum up to 14 000 cm^{-1}

The band centers and relative intensities for 22 bands which could be assigned to the CH stretching and bending system, between 1370 and 14 000 cm^{-1} are collected in Table II (column "observed"). These data have been used in a global least squares fit using Marquardt's algorithm[48] with seven parameters of the effective Hamiltonian. The best fit parameters are shown in Table III. The agreement of the model predictions and the experiment can be seen from the relevant columns in Table II. The root mean square deviation is 1.9 cm^{-1}. Although this is much larger than the possible experimental error, it is an outstandingly good fit in view of the simplicity of the model and the large frequency range considered. Small corrections by the introduction of higher order terms would bring the fit to the experimental accuracy, but we do not attach much significance to the higher order parameters and we thererefore present here only the results for the simple model.

The values of the anharmonic stretching oscillator constants $\tilde{\nu}_s'$ and x_{ss}' have been repeatedly evaluated before without taking the Fermi resonances into account. It is quite clear that the present, reliable values are quite different from these previous determinations. The bending frequency $\tilde{\nu}_b'$ is in essential agreement with the result of Ref. 21, when one takes into account the different definitions of the constants and the fact that a parameter from such a global fit has a somewhat different meaning from the parameter determined from just one band. The value of x_{sb}' is interestingly similar to the values found for the acetylenes.[46] It can be simply related to a decrease of the effective bending frequency with increasing CH-bond extension or vibrational excitation in the adiabatic picture.[18,46] It must be stressed that without a global understanding of the complete Fermi resonance system there would be no way to determine this parameter correctly from an individual sum or difference or hot band transition involving ν_s and ν_b. The absolute values of x_{bb}' and g_{bb}' are small and therefore relatively less accurate, whereas $|k_{sbb}|$ again is very large, indeed. Its sign is not available from the fit, but can be fixed by means of qualitative considerations. In the case of CD_3H, the sign is available from *ab initio* calculations.[18]

The Fermi resonance parameter k_{sbb} is central for the present model. It is related to the Fermi resonance matrix element for the $N = 1$ dyad through $|W_{(1)}| = |k_{sbb}|/\sqrt{2} = 75$

$$H^3 = \begin{array}{c} \begin{matrix} |3,0,0\rangle & |2,2,0\rangle & |1,4,0\rangle & |0,6,0\rangle \end{matrix} \\ \begin{pmatrix} H_{11}^3 & -\sqrt{3/2}\,k_{sbb} & 0 & 0 \\ -\sqrt{3/2}\,k_{sbb} & H_{22}^3 & -2k_{sbb} & 0 \\ 0 & -2k_{sbb} & H_{33}^3 & -\frac{3}{\sqrt{2}}k_{sbb} \\ 0 & 0 & -\frac{3}{\sqrt{2}}k_{sbb} & H_{44}^3 \end{pmatrix} \end{array} \begin{matrix} |3,0,0\rangle \\ |2,2,0\rangle \\ |1,4,0\rangle \\ |0,6,0\rangle \end{matrix}$$

$$\begin{pmatrix} 8684 & +130 & 0 & 0 \\ +130 & 8526 & +213 & 0 \\ 0 & +213 & 8310 & +226 \\ 0 & 0 & +226 & 8036 \end{pmatrix}$$

FIG. 3. Structure of the Fermi resonance Hamiltonian for the $N = 3$ polyad. (a) General form. (b) Numerical values in cm^{-1} units from the best fit.

TABLE II. Comparison between experiment and the tridiagonal Fermi resonance model.

State		Observed		Calculated			
N	j	$\tilde{\nu}/cm^{-1}$	Notes	$\tilde{\nu}/cm^{-1}$	g(expt)[l]	g(calc)	Weight
(A) A_1 Polyads							
1	1	3 035.5	a	3 036.4	0.954	0.944	1.0
	2	2 710.2	b	2 711.1	0.046	0.056	1.0
2	1	5 959.4	c	5 961.5	0.6	0.81	1.0
	2	5 710.4	d	5 709.5	0.4	0.18	1.0
	3	5 337		5 339.2	weak	0.01	0.5
3	1	8 792.7	e	8 792.2	0.52	0.53	1.0
	2	8 589.3	f	8 589.3	0.45	0.43	1.0
	3	8 286.0		8 285.5	0.03	0.04	1.0
	4	7 890		7 887.7	weak	0.001	1.0
4	1	11 563	g	11 563.2	0.18	0.17	1.0
	2	11 347	h	11 344.5	0.66	0.63	1.0
	3	11 109	i	11 107.7	0.16	0.19	1.0
	4	...		10 774.1	...	0.01	...
	5	...		10 358.8	...	0.0002	...
5	2	14 002.8	j	14 009.0	weak	0.35	0.5
(B) E Polyads							
(1/2)	1	1 377.85	k	1 375.8	1.0	1.0	1.0
(3/2)	1	4 400		4 400.3	0.99	0.90	1.0
	2	4 044		4 044.3	(0.01)	0.10	0.5
(5/2)	1	7 322		7 320.6	0.75	0.72	1.0
	2	7 018		7 020.9	0.25	0.27	1.0
	3	...		6 632.0	...	0.01	...
(7/2)	1	10 155.9		10 153.3	0.45	0.44	1.0
	2	9 881.9		9 883.1	0.49	0.48	1.0
	3	9 550.0		9 551.8	0.06	0.08	1.0
	4	...		9 141.5	...	0.003	...
(9/2)	2	12 639.6	j	12 637.4	weak	0.54	0.5

[a] See Ref. 23; we find $G = 0.132$ (pm)^2 for this band.
[b] Reference 25 has 2710.2 and Ref. 57 gives 2710.26.
[c] Reference 26 gives 5959.46 and Ref. 24 gave 5978 cm^{-1}. We find $G = (2 \pm 0.4) \times 10^{-4}$ (pm)^2 for this band.
[d] Reference 24 gave 5728 cm^{-1}.
[e] Reference 24 gave 8792.75 cm^{-1}; we find $G = (3 \pm 1) \times 10^{-5}$ (pm)^2 for this band.
[f] Reference 24 gave 8589.3 cm^{-1}.
[g] Reference 24 gave 11 563.4 cm^{-1}.
[h] Reference 24 gave 11 347.2 cm^{-1}; we find $G = (2.4 \pm 1) \times 10^{-6}$ (pm)^2 for this band.
[i] Reference 24 gave 11 109.2 cm^{-1}.
[j] Preferred value taken from Ref. 24.
[k] Preferred value taken from Ref. 21.
[l] For one component in each band system absolute values of G are given in the notes.

cm^{-1} from the present results. This matrix element had been determined previously[26] as 111 cm^{-1}. This is much too large, due to the fact that in this estimate the unknown zero order position of $2\nu_b(A_1)$ was involved. As was pointed out already in Ref. 23 a somewhat better approach is possible by using the band intensities of the Fermi dyad and assuming that the zero order intensity of the bending overtone is small. We have measured

$$G((1)_1) = (0.132 \pm 0.02)(\text{pm})^2,$$
$$G((1)_2) = (0.0063 \pm 0.002)(\text{pm})^2.$$

TABLE III. Parameters of the Fermi resonance model.

$\tilde{\nu}_s' =$	3079.8 cm^{-1}
$\tilde{\nu}_b' =$	1377.8 cm^{-1}
$x_{ss}' =$	− 61.7 cm^{-1}
$x_{sb}' =$	− 28.6 cm^{-1}
$x_{bb}' =$	− 6.5 cm^{-1}
$g_{bb}' =$	4.5 cm^{-1}
$k_{sbb} = (\pm)^a$	106.1 cm^{-1}

[a] See discussion in the text for the sign, which cannot be determined directly.

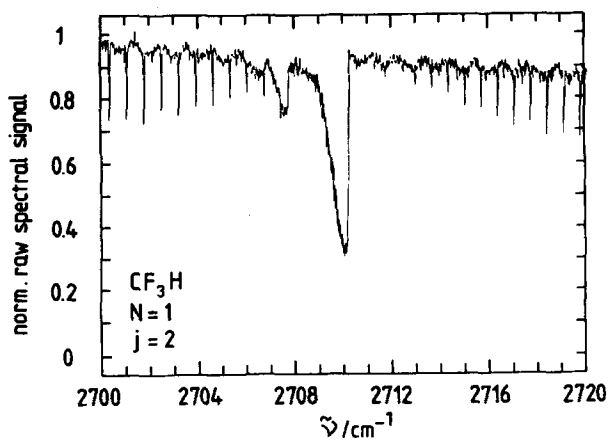

FIG. 4. Central portion of the raw FTIR spectrum of the $(1)_2$ band ($P = 260$ Pa, $l = 7$ m, resolution 0.02 cm^{-1}). The hot band at 2707.5 cm^{-1} is discussed in Sec. III F.

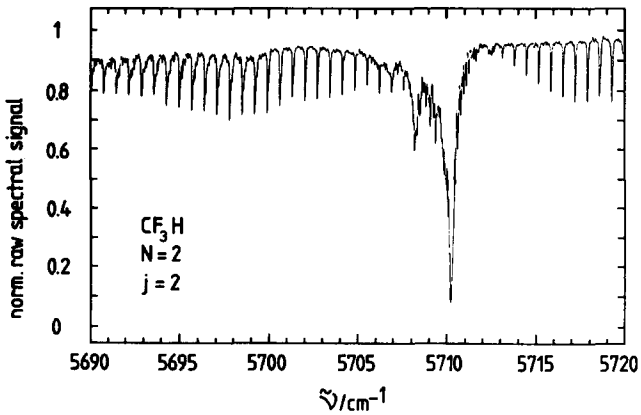

FIG. 5. Central portion of the raw FTIR spectrum of the $(2)_2$ band ($P = 1.4$ kPa, $l = 14.5$ m, resolution 0.03 cm^{-1}). The hot band at 5708 cm^{-1} is discussed in Sec. III F.

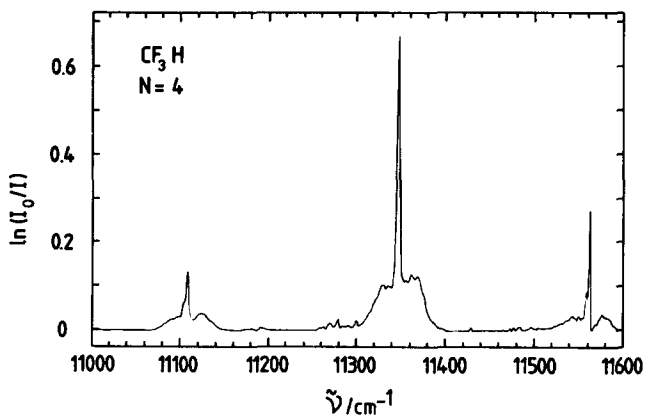

FIG. 7. Survey spectrum of the $N = 4$ polyad ($P = 0.87 \times 10^5$ Pa, $l = 22.5$ m). See the discussion in the text.

From these values one estimates $|W| = 68\ cm^{-1}$, in better agreement with the global fit. In order to judge the accuracy of the result for k_{sbb} in the global fit, we have chosen several fixed values for k_{sbb}, adjusting all the other parameters in a least squares fit. It is found that a change of k_{sbb} by $\pm 15 cm^{-1}$ leads to poor model predictions. These boundaries can be considered to specify the limits within which physically reasonable values for k_{sbb} may be possible. This result is also established by using fits involving higher order terms in the Hamiltonian. Figure 4 shows the central portion of the $(1)_2$ component at moderate resolution, which shows a hot band and otherwise largely unperturbed rotational J structure.

The two strong components of the $N = 2$ polyad are shown in Figs. 5 and 6. The rotational structure will be further discussed below. The intensities of these two bands have been measured to be

$$G((2)_1) = (2 \pm 0.4) \times 10^{-4} (pm)^2,$$

$$G((2)_2) = (1.3 \pm 0.3) \times 10^{-4} (pm)^2.$$

Compared to the model prediction in Table II the intensity ratio is rather surprising and is explained by an appreciable zero order intensity of the $|1, 2,0\rangle$ state. The third very weak component at 5337 cm^{-1} could be identified by means of the model prediction.

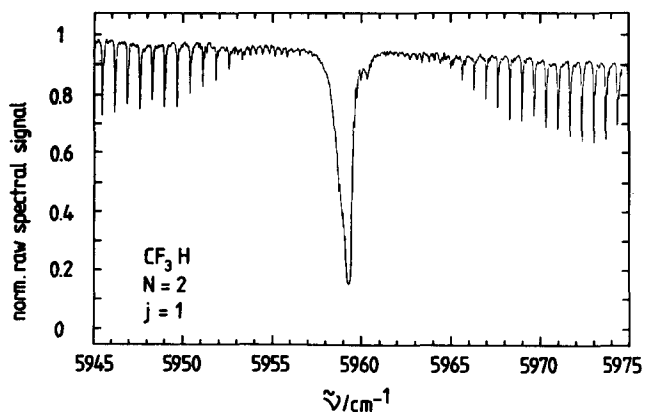

FIG. 6. The spectrum of the $(2)_1$ band (conditions as in Fig. 5). Note the perturbations for the low J lines in the P and R branches. The hot band is hidden in the Q branch.

Figure 7 shows as a last example a survey spectrum of the three prominent parallel band members $(4)_1$, $(4)_2$, $(4)_3$ of the $N = 4$ polyad. This figure illustrates that at this level the most intense band in the system is no longer at the high frequency end but rather in the middle. This effect can be understood with the model parameters of Table III and the graphical representation of the diagonal part of the Hamiltonian of the A_1 polyads in Fig. 8. This figure shows how the zero order energies of the excited bending vibrational states move upwards compared to the pure stretching state, because of its larger anharmonicity. (The zero of energy has

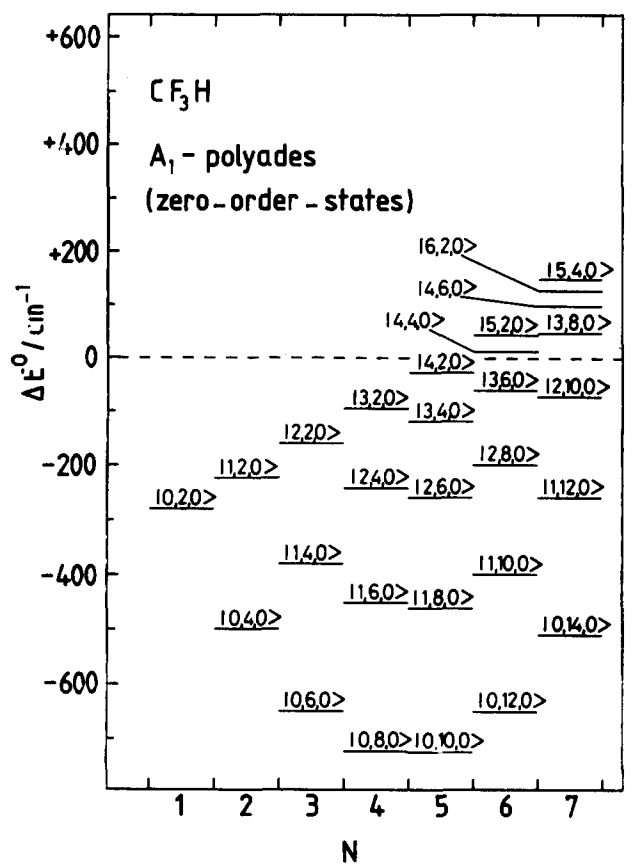

FIG. 8. Reduced energy plot for the zero order states $|v_s, v_b, l_b\rangle$. The zero of energy is redefined at each N to be the energy of the $|v_s, 0, 0\rangle$ state, which is not shown explicitly. The coupled states for one polyad appear as one column with a given N.

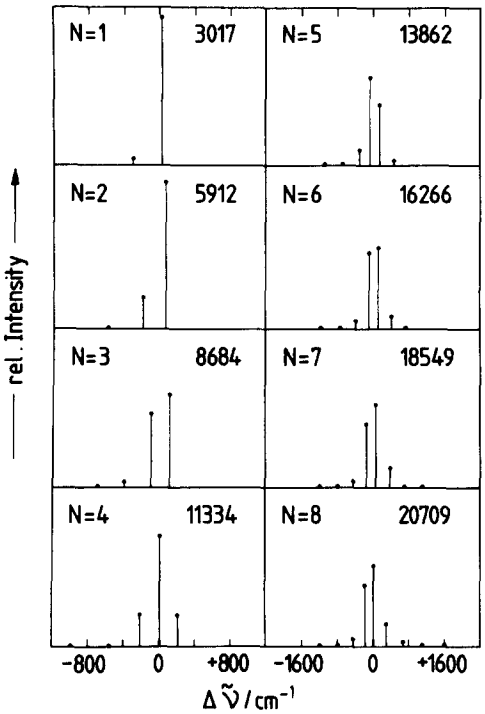

FIG. 9. Survey of vibrational band positions and intensities (heights of the sticks) predicted from the model Hamiltonian for polyads with N between 1 and 8. The zero of the energy for each polyad is given by the number (cm^{-1} units) shown as insert. Note the different energy scales for the polyads with $N<4$ and $N>4$.

been set at the pure stretching states.) At some value of N the zero order energy of $|N, 0, 0\rangle$ is smaller than that of $|N-1, 2, 0\rangle$, which qualitatively accounts for the intensity distribution. More quantitatively the predicted trends in vibrational band intensities with increasing N are shown in Fig. 9 for bands up to 20 000 cm^{-1}. The switchover at $N=4$ and the complete redistribution for even higher energies is easily visualized. These trends are also observed in $(CF_3)_3CH$, where bands with N up to 6 were observed.[17] In the case of CF_3H only one band with $N=5$ is so far available from Ref. 24, which can be assigned as $(5)_2$ at 14 002.8 cm^{-1}. The bands shown in Fig. 9 can be taken as predictions from the model for future studies by more sensitive spectroscopic techniques, such as photoacoustic laser spectroscopy.[7] In the case of $(CF_3)_3CH$[17] and CD_3H[18] the model was found to give good predictions for higher energy overtones beyond the values observed in the infrared.

The bands of the E polyads (half integral N) can be assigned because of their characteristic perpendicular structure with the well established value $\zeta_b = 0.985$ for the Coriolis coupling constant.[21] The band structures with $\zeta_6 = -0.806$[20,30] and $\zeta_5 = 0.733$ (estimated from the sum rule[49] in our work before the recent accurate experimental value of 0.718 was available[22]) are significantly different from the E-bending polyad bands. Figure 10 shows a survey spectrum of the $N=7/2$ polyad, in which three bands with $\zeta = 0.985$ appear. The fourth expected band at 9141.5 cm^{-1} is too weak for observation, at present. The assignment of the polyad bands is established beyond doubt from the model prediction [see Table II B] and the rotational analysis given below. There appear two further weak bands in Fig. 10 which show a perpendicular band structure corresponding to $\zeta_5 = 0.72$. The appearance of weak combination bands with the CF_3 stretching vibration is not entirely unexpected but nevertheless interesting. The bands are tentatively assigned as $(3)_2 + (\nu_2/\nu_5)$ at 9730 cm^{-1} and as $(3)_1 + (\nu_2/\nu_5)$ at 9940 cm^{-1} (ν_2/ν_5 occurs as a Coriolis coupled pair of bands).

The analysis and assignment of further bands in the E-polyade systems proceeds similarly and will not be discussed in detail here. Rather we shall present some examples of the detailed rotational analyses of the high resolution spectra, which are an important piece of evidence for the definite assignments of the polyad bands.

E. Sample rotational analyses

The complete rotational analysis of 22 bands, which often show many local rovibrational perturbations, is a considerable task, which has not yet been completed in the four years our study has been underway. We shall present here just a few examples at higher resolution, which show how our assignments have been backed by the rotational structure of the bands and which give some additional insight in the molecular parameters for the bands involved in the Fermi resonance.

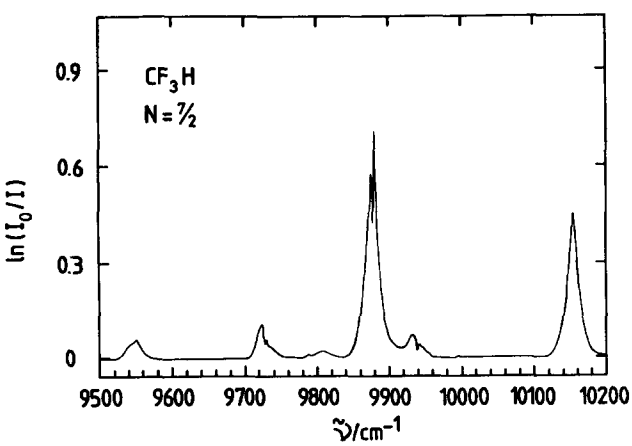

FIG. 10. Survey spectrum of the $N=(7/2)$ polyad ($P=0.87\times10^5$ Pa, $l=15.5$ m).

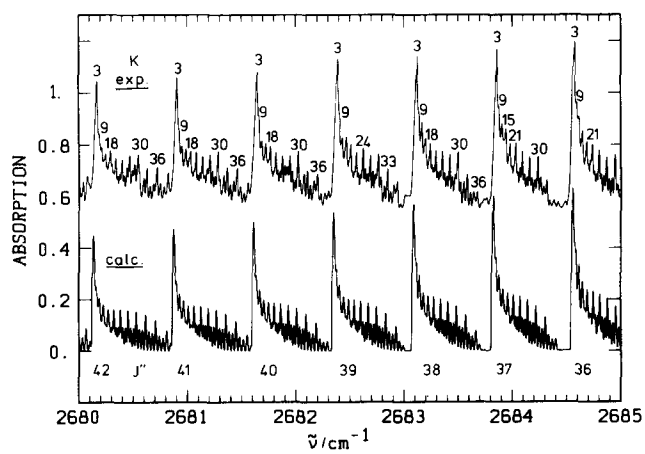

FIG. 11. Portion of the P branch of the $(1)_2$ band ($P=1$ kPa, $l=5.75$ m, effective resolution 0.014 cm^{-1}). The lower curve is the simulated, the upper curve the experimental spectrum (see also the detailed discussion in the text).

TABLE IV. Least squares parameters for the $(1)_2$ component.[b]

	Fit(i)[d]		Fit (ii)[e]	
Constant	Ground state[a]	$(1)_2$	Ground state	$(1)_2$
$\tilde{\nu}_0/\text{cm}^{-1}$	0	2710.210	0	2710.210
C/cm^{-1}	0.189 25	0.189 055 6(8)	...	...
B/cm^{-1}	0.345 201 05	0.344 515 1(6)	0.345 194(10)	0.344 507(10)
D_J/cm^{-1}	3.779×10^{-7}	$3.808(3)\times10^{-7}$	$3.77(7)\times10^{-7}$	$3.80(7)\times10^{-7}$
D_{JK}/cm^{-1}	-6.0375×10^{-7}	$-6.057(5)\times10^{-7}$	$-6.2(4)\times10^{-7}$	$-6.3(4)\times10^{-7}$
D_K/cm^{-1}	3.72×10^{-7}	$3.691(5)\times10^{-7}$	...	...
$(\Delta C-\Delta B)^c/\text{cm}^{-1}$	...	...	$4.92(1)\times10^{-3}$	
$(D'_K-D''_K)/\text{cm}^{-1}$	...	...	$-3.1(5)\times10^{-9}$	

[a] For the ground state constants see Refs. 21 and 29–32.
[b] The numbers in parenthesis give the standard deviations in units of the last digit.
[c] $\Delta B = B' - B''$, $\Delta C = C' - C''$.
[d] Ground state constants fixed.
[e] Ground state constants adjusted in the fit.

Figure 4 shows the central portion of the parallel band corresponding to the $(1)_2$ component, which shows essentially unperturbed *PQR* structure, with unresolved *K* structure at this resolution. This band has also been recorded at an effective resolution of 0.014 cm^{-1}, without pressure broadening, where the *K* structure could be largely resolved. Figure 11 shows a part of the *P* branch. The spectrum was calculated using the term formula including some of the higher order terms for both the ground and excited states:

$$F(\tilde{\nu}_0, J, K) = \tilde{\nu}_0 + B\cdot J(J+1) + (C-B)K^2 - D_J J^2(J+1)^2 - D_{JK}J(J+1)K^2 - D_K K^4. \quad (22)$$

A total of 448 lines was assigned and introduced in two nonweighted least squares fits. In fit (i) the ground state constants were fixed at the values known from microwave spectroscopy, in fit (ii) all constants entering the relevant equations for transition energies were adjusted to a best fit. The standard deviation of both fits was 1.6×10^{-3} cm^{-1}, approximately a tenth of the resolution. The lines with $K = 30$ to 32 were all found to be weakly perturbed. Table IV summarizes the constants obtained from the two fits. The uncertainty in the band center at (2710.210 ± 0.006) cm^{-1} is mainly due to the uncertainty in the calibration lines of HCl (± 0.006 cm^{-1}).[36] Our data are more accurate but consistent with the values of $\nu_0 = 2710.23$ cm^{-1} and $B' = 0.344\,49$ cm^{-1} determined from lower resolution data by Costain.[31]

The fine structure of the two strong components $(2)_1$ and $(2)_2$ at 5959 and 5710 cm^{-1} shows some interesting effects (see Figs. 5 and 6 for intermediate resolutions traces). The *K* structure in both bands in *P* and *R* branches is strongly blue shaded, due to the large value of $[(C'-C'')-(B'-B'')]$. The 2_1 band shows a perturbation for the low *J* values. These seem to be "missing" in Fig. 6 (compare Fig. 5), because up to $J'' = 9$ each line is split into two components. This may indicate an additional very weak Fermi resonance, which is tuned out of resonance as *J* increases because of the different rotational constants of the states involved in the resonance. Such perturbations are fairly typical but they do not, of course, in any substantial way affect the analysis of the very strong resonances. A least squares analysis does not lead to very well determined centrifugal distortion constants, which are given as preliminary values in Table V. An analysis of further, very high resolution spectra of these bands is in progress.[19]

TABLE V. Summary of rotational constants and band centers.

State	Band center $\tilde{\nu}_0/\text{cm}^{-1}$	C/cm^{-1}	B/cm^{-1}	Remarks
1_2	2 710.210	0.189 055 6	0.344 515 1	see Table IV
2_1	5 959.443	0.189 1	0.344 75	this work[a]
2_1	5 959.46	...	0.344 89	Ref. 50
2_2	5 710.487	0.189 62	0.344 65	this work[b]
3_1	8 792.70	...	0.344 315	this work[c]
3_1	8 792.75	...	0.344 40	Ref. 24
3_2	8 589.28	...	0.344 23	Ref. 24
$(7/2)_1$	10 155.9	0.188 25	0.343 6	this work
$(7/2)_2$	9 881.9	0.189 00	0.341 0	this work

[a] Preliminary centrifugal constants:
$D_J = 3.67\times10^{-7}\,\text{cm}^{-1}$, $D_{JK} = -2.9\times10^{-7}\,\text{cm}^{-1}$, $D_K = -3.1\times10^{-7}\,\text{cm}^{-1}$.
[b] $D_J = 2.7\times10^{-7}\,\text{cm}^{-1}$, $D_{JK} = -8.7\times10^{-7}\,\text{cm}^{-1}$, $D_K = 7.7\times10^{-7}\,\text{cm}^{-1}$.
[c] $D_J = 3.69\times10^{-7}\,\text{cm}^{-1}$.

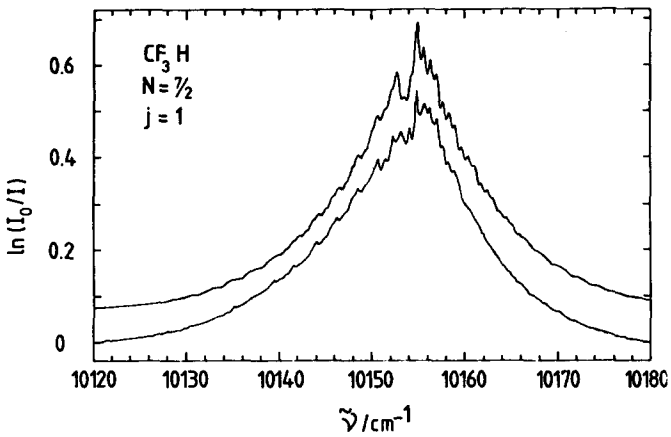

FIG. 12. Spectrum of the $(7/2)_1$ band ($P = 0.87 \times 10^5$ Pa, $l = 15.5$ m, resolution 0.05 cm^{-1}). The upper curve is calculated with $\zeta = 0.985$ and the other constants as discussed in the text.

Figures 12 and 13 show examples from the E-band systems, $(7/2)_1$ and $(7/2)_2$ under pressure broadened conditions (about 0.4 cm^{-1} FWHM for 0.85×10^5 Pa from the fit to the spectra). These spectra were fitted with the low order term formula for degenerate vibrational states:

$$F(\tilde{\nu}_0, J, K) = \tilde{\nu}_0 + BJ(J+1) + (C - B)K^2 \pm 2C\zeta K. \quad (23)$$

The appearance of the bands depends importantly upon ζ. The bands can be well fitted with $\zeta = 0.985$, as determined for ν_b.[21] In the fit the upper state rotational constants were adjusted as well and each line was convoluted with a Lorentzian of 0.4 cm^{-1} width for the pressure broadening. The band at 9882 cm^{-1} had been observed and assigned by Bernstein and Herzberg.[24] The data from the rotational analyses are collected in Table V, including also some previous results. It should be clear from the examples that the band assignment can be made without ambiguity using the rotational structure and the predictions from the Fermi resonance model. More details about the rotational structure and constants, which are consistent with the Fermi resonance model, will be presented elsewhere.[19]

F. Hot bands in Fermi resonance

Numerous hot-band, sum and difference transitions are observed in the IR spectra of CF_3H between 900 and 14 000

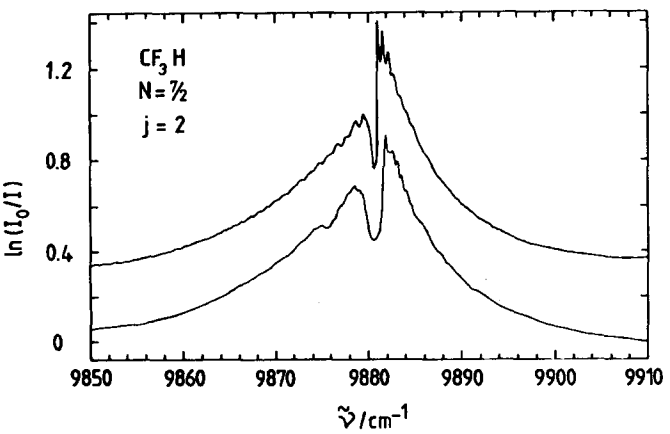

FIG. 13. Spectrum of the $(7/2)_2$ band (see Fig. 12 and the text for details).

TABLE VI. Summary of approximate anharmonicity constants.

Constant	x/cm^{-1}
$x'_{11} = x'_{ss}$	− 61.7
$x'_{14} = x'_{sb}$	− 28.6
x_{23}	− 1.6
x_{24}	− 1.1
x_{26}	− 2
x_{33}	− 0.4[a]
x_{35}	− 5.5
x_{36}	− 0.14[a]
$x'_{44} = x'_{bb}$	− 6.5
x_{46}	− 1.25
x_{56}	− 8
x_{66}	− 0.15[a]

[a] Accurate values from Ref. 20.

cm^{-1}. Table VI gives a summary of anharmonic constants (approximate values only, because in most cases accurate band centers have *not* been determined from a detailed rotational least squares fit). We shall discuss here in more detail only one aspect, namely how the position of certain hot bands is affected by the Fermi resonance between $\nu_s \equiv \nu_1$ and $\nu_b \equiv \nu_4$. Two examples are chosen: (i) The hot bands arising from the separate, low frequency fundamental $\nu_6 = 508$ cm^{-1}, which acts as a "spectator" in transitions with the ν_s, ν_b polyades. (ii) The hot bands arising from the "active participant" ν_b within this Fermi resonance system.

We have noted the occurrence of hot bands with ν_6 in our discussion of several spectra in Sec. III D (see Figs. 4, 5, and 7). They have an intensity of about 17% of the cold bands at room temperature. Table VII gives a summary of the observed transitions in terms of the frequency shift with respect to the cold band. Using the diagonal elements of the Hamiltonian in Eq. (3) with $x_{16} \simeq 0$ cm^{-1} and $x_{46} \simeq -1.25$ cm^{-1}, one can calculate the positions of the hot bands, assuming that the Fermi resonance matrix elements are in first order unaffected by the excitation of ν_6. The results of such a model are shown in the column $\Delta\tilde{\nu}_{th}$. Although the agreement does not seem to be too good, one must remember that we are considering now small shifts, using a Hamiltonian which was found to be accurate only on the scale of the large displacements observed in the Fermi resonance. More interesting than the small deviations between experiment and theory, which are caused in some cases by identified, although not assigned local perturbations, are the trends compared to the *zero order shifts* $\Delta\tilde{\nu}^0$, which are calculated just from the diagonal part of the Hamiltonian in Eq. (3), without diagonalizing the Fermi resonance. One can clearly see how the Fermi resonance tends to mix the anharmonic shifts. This mixing of anharmonic shifts involving a spectator low frequency vibration can be understood on very similar grounds as the mixing of rotational constants in Fermi resonance.[19] A more detailed discussion is hampered at present by the lack of relative accuracy in the experimental data for the hot bands of ν_6 and by the relatively large influence of local perturbations on such small shifts.

The hot bands arising from $\nu_4 = \nu_b$ show much larger shifts and are therefore not subject to the difficulties mentioned above. These bands have an intensity of about 0.3% of

TABLE VII. Shifts for hot bands in Fermi resonance involving ν_6 as lower state of the transition.

Hot band (spectroscopic notation)	Cold band	Shift of hot band minus cold band		
		$\Delta\tilde{\nu}_{expt}/cm^{-1}$	$\Delta\tilde{\nu}_{th}/cm^{-1}$	$\Delta\tilde{\nu}^0/cm^{-1}$
$2\nu_4+\nu_6-\nu_6$	$(1)_2$	−2.5	−2.5	−2.5
$2\nu_1+\nu_6-\nu_6$	$(2)_1$	(small)[a]	−0.4	0.0
$\nu_2+2\nu_4+\nu_6-\nu_6$	$(2)_2$	−2.75[a]	−2.4	−2.5
$3\nu_1+\nu_6-\nu_6$	$(3)_1$	−1.2	−1.3	0.0
$2\nu_1+2\nu_4+\nu_6-\nu_6$	$(3)_2$	−3.25	−2.7	−2.5
$\nu_1+4\nu_4+\nu_6-\nu_6$	$(3)_3$	−5.0	−4.6	−5.0
$6\nu_4+\nu_6-\nu_6$	$(3)_4$	−5.0	−6.8	−7.5
$4\nu_1+\nu_6-\nu_6$	$(4)_1$	−3	−2.9	0
$3\nu_1+2\nu_4+\nu_6-\nu_6$	$(4)_2$	(small)	−2.2	−2.5
$2\nu_1+4\nu_4+\nu_6-\nu_6$	$(4)_3$	−4.5	−4.3	−5.0

[a] Additional perturbation see Sec. III E.

the cold bands at room temperature and can thus be measured if they occur in not too crowded regions of the spectrum. However, they can also be obtained very accurately from combination differences. Table VIII gives a comparison of the ν_4 hot band shifts with shifts calculated from the Fermi resonance model and from the zero order Hamiltonian, Eq. (3). Our Fermi resonance notation replaces here the approximate spectroscopic notation, for example $(3/2)_1$–$(1/2)_1$, corresponds to $(\nu_1+\nu_4-\nu_4)$, etc. Although the absolute errors in the calculated shifts still are of the order of a couple of cm^{-1}, the relative errors are now meaningfully small, indicating the essential agreement of the model with experiment. On the other hand, the calculated zero order shifts $\Delta\tilde{\nu}^0$ have no obvious relationship to experiment, apart from an accidental coincidence for the $(3)_2$ band. As we have already pointed out elsewhere, the proper understanding of the homogeneous (e.g., Fermi resonance) and inhomogeneous (e.g., hot band) vibrational structure in the infrared absorption of polyatomic molecules is of considerable interest for the theory of IR-laser excitation of polyatomic molecules.[16,51]

G. Effective Hamiltonian and time-dependent vibrational dynamics for the Fermi resonance

Having established the Hamiltonian for the coupled CH-stretching and bending vibrations experimentally (Table III), we can calculate the desired time evolution for vibrational motion in the absence of external perturbations using the time evolution matrix (for each block of **H**, represented here in energy units):

$$\mathbf{U}(t)=\exp(-2\pi i\mathbf{H}t/h). \tag{24}$$

U solves the time dependent Schrödinger equation for the amplitude vector **b**, the Liouville–von Neumann equation for the density matrix P, or the Heisenberg equations of motion for the matrix representation **Q** of an observable (operator) according to Eqs. (25) to (27):

$$\mathbf{b}(t)=\mathbf{U}(t)\mathbf{b}(0), \tag{25}$$

$$\mathbf{P}(t)=\mathbf{U}(t)\mathbf{P}(0)\mathbf{U}^+(t), \tag{26}$$

$$\mathbf{Q}(t)=\mathbf{U}^+(t)\mathbf{P}(0)\mathbf{U}(t). \tag{27}$$

As an example we show in Fig. 14 the time evolution of the populations $|b_k|^2$ of spectroscopic zero order states, when initially the state $|v_s=3, v_b=0, l_b=0\rangle$ is populated (i.e., the Hamiltonian applies to the $N=3$ polyad). The experimental preparation of this state should be possible, in principle, although not easily so in practice, by extremely wide band, short pulse excitation ($\simeq$0.01 ps) of this polyad disregarding weak features and absorptions in the wings of the spectral profile of the pulse. Figure 14 illustrates how the state $|1\rangle=|v_s=3, v_b=0, l_b=0\rangle$ rapidly decays within about 0.1 ps, the states $|2\rangle=|v_s=2, v_b=2, l_b=0\rangle$ and $|3\rangle=|v_s=1, v_b=4, l_b=0\rangle$ being populated to about 70% and 40% during this period. Even the state $|4\rangle=|0, 6, 0\rangle$ is populated with a few percent in this energy redistribution. This shows how extensively energy can flow between the CH-stretching and bending degrees of freedom due to the tridiagonal Fermi resonance. The *initial* population of the states $|2\rangle$, $|3\rangle$, and $|4\rangle$ occurs sequentially, as suggested by the coupling matrix. On the other hand, the

TABLE VIII. Shifts for hot bands involving ν_4 as lower state (Fermi resonance notation see the text).

Hot band	Cold band	Shift of hot band minus cold band		
		$\Delta\tilde{\nu}_{expt}/cm^{-1}$	$\Delta\tilde{\nu}_{th}/cm^{-1}$	$\Delta\tilde{\nu}^0/cm^{-1}$
$(3/2)_1$–$(1/2)_1$	$(1)_1$	−12.9	−11.9	−28.6
$(3/2)_2$–$(1/2)_1$	$(1)_2$	−43.6	−42.6	−26.0
$(5/2)_1$–$(1/2)_1$	$(2)_1$	−14.8	−16.6	−57.2
$(5/2)_2$–$(1/2)_1$	$(2)_2$	−69.8	−64.4	−54.6
$(7/2)_1$–$(1/2)_1$	$(3)_1$	−13.7	−14.7	−85.8
$(7/2)_2$–$(1/2)_1$	$(3)_2$	−84.8	−82.0	−83.2
$(7/2)_3$–$(1/2)_1$	$(3)_3$	−113.4	−109.5	−80.6
$(9/2)_2$–$(1/2)_1$	$(4)_2$	−84.8	−82.9	−111.8

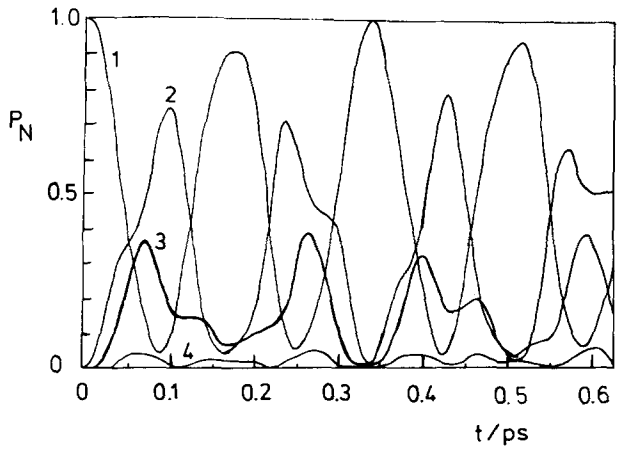

FIG. 14. Time evolution for the populations of states interacting in the $N = 3$ polyad calculated with the spectroscopic Fermi resonance Hamiltonian and the initial condition $p(|3, 0, 0\rangle) = 1$. See also the text for the detailed discussions.

times of substantial redistribution are about equal (< 0.1 ps) for all three states. The time evolution is oscillatory because of the few states which are effectively coupled on this short time scale.[52] There are strong selection rules, which allow one quantum jumps for the stretching vibration and two quantum jumps for the bending vibration. Finally, our Hamiltonian gives a correct description of the short time evolution only. In order to predict the evolution for longer times ($\gtrsim 1$ ps) a more detailed understanding of the small perturbations in the spectra at high resolution is necessary.

IV. CONCLUSIONS

(i) In the CH-overtone spectrum of CF_3H a complex vibrational multiplet of bands appears, instead of one band which might naively be expected for a single local or normal mode state. This observation by itself is important for the often suggested, simple interpretation of overtone spectra of molecules with several different CH oscillators in terms of local mode models disregarding the true multiplet structure even for one mode.[53]

(ii) The observed structures can be explained by means of a tridiagonal Fermi resonance Hamiltonian, which accounts quantitatively for the intensities and positions of the numerous (22) observed bands. The assignments can be made unambiguously, making use of the rotational structure of the bands. A few further, weaker bands arise from combination with the CF_3 stretching vibrations. The Hamiltonian has been used to predict the structure of the high overtone spectra in the visible which are measurable by photoacoustic spectroscopy.

(iii) The tridiagonal, multiple Fermi resonance reported here for the CF_3H molecule is by no means accidental, but seems to be a universal dynamical property of the isolated alkyl-CH chromophore. We have evaluated this in detail already for $(CF_3)_3CH$,[14,17], CD_3H[18,54] and further molecules.[19] It can be established also by *ab initio* calculations.[18] There are also several instances in the literature, where two level Fermi resonances have been invoked, where, however, there seems to be definite evidence from reconsideration of the published data that the tridiagonal resonance occurs (for example, in $CHCl_3$ and $CHBr_3$.[55]) It seems to us that the relevant couplings are also of great importance in spectra which do not involve the isolated CH chromophore, but several coupled CH oscillators, although these spectra are more difficult to interpret.[56]

The present, unambiguous proof of the occurrence of a tridiagonal Fermi resonance structure *may* perhaps be relevant also in relation to the theoretical interpretation of the overtone linewidths in benzene given by Sibert, Reinhardt, and Hynes.[11] These authors have invoked Fermi-coupled states as doorway states for the final decay giving widths of the order of 100 cm^{-1}. As no definite structure from the Fermi resonances can as yet be assigned in these broad bands, the interpretation must remain conjectural.

(iv) The tridiagonal Fermi resonance Hamiltonian can be used to describe the time dependent flow of energy between CH stretching and bending vibrational modes. Rather complete oscillatory redistribution is observed for high levels of excitation on time scales of 0.1 ps. This implies a complete breakdown of the vibrationally adiabatic approximation for the isolated alkyl-CH-chromophore, in contrast to the acetylenic CH chromophore, where the adiabatic decoupling between the stretching and bending motions was found to hold up to high levels of excitation.[46] We have thus a well defined structural element, in which the relationship between molecular structure and vibrational redistribution has been identified and understood on the basis of a simple Hamiltonian.

ACKNOWLEDGMENTS

Discussions with and help from Marius Lewerenz are gratefully acknowledged. Don Lupo carefully read and criticized the manuscript. Our work is financially supported by the Schweizerischer Nationalfonds. The initial phase of this work was funded by the DFG through SFB 93, project C7, and by the Fonds der Chemischen Industrie.

[1] G. Herzberg, *Molecular Spectra and Molecular Structure* (Van Nostrand Reinhold, New York,1945 and 1966), Vol. II and Vol. III.
[2] S. A. Rice, in *Excited States*, edited by E. C. Lim (Academic, New York, 1975).
[3] M. Quack and J. Troe, Int. Rev. Phys. Chem. **1**, 97 (1981).
[4] M. Quack, in *Energy Storage and Redistribution in Molecules*, edited by J. Hinze (Plenum, New York 1983), p. 493.
[5] C. S. Parmenter, Faraday Discuss. Chem. Soc. **75**, 7 (1983).
[6] A. H. Zewail, Acc. Chem. Res. **13**, 360 (1980); Faraday Discuss. Chem. Soc. **75**, 315 (1983).
[7] M. C. Chuang, J. E. Baggott, D. W. Chandler, W. E. Farneth, and R. N. Zare, Faraday Discuss. Chem. Soc. **75**, 301 (1983); T. R. Rizzo, C. Hayden, and F. F. Crim, *ibid.* **75**, 223 (1983); R. G. Bray and M. J. Berry, J. Chem. Phys. **71**, 4909 (1979); G. A. West, R. P. Mariella, J. A. Pete, W. B. Hammond, and D. F. Heller, *ibid.* **75**, 2006 (1981); D. J. Nesbitt and S. R. Leone, Chem. Phys. Lett. **87**, 123 (1982).
[8] C. Kolmeder, W. Zinth, and W. Kaiser, Chem. Phys. Lett. **91**, 323 (1982); B. Kopainsky and W. Kaiser, *ibid.* **66**, 39 (1979); J. P. Maier, A. Seilmeier, and W. Kaiser, **70**, 591 (1980); A. Laubereau and W. Kaiser, Rev. Mod. Phys. **50**, 607 (1978); A. Fendt, S. F. Fischer, and W. Kaiser, Chem. Phys. **57**, 55 (1981).
[9] C. Tric, Chem. Phys. **14**, 189 (1976); S. Mukamel and R. E. Smalley, J. Chem. Phys. **73**, 4156 (1980); D. F. Heller and S. Mukamel, *ibid.* **70**, 463 (1979).
[10] R. T. Lawton and M. S. Child, Mol. Phys. **37**, 1799 (1979); **44**, 709 (1981); E. L. Sibert, J. T. Hynes, and W. P. Reinhardt, J. Chem. Phys. **77**, 3595 (1982); L. Halonen, M. S. Child, and S. Carter, Mol. Phys. **47**, 1097 (1982).

[11]E. L. Sibert, W. P. Reinhardt, and J. T. Hynes, Chem. Phys. Lett. **92**, 455 (1982); P. J. Nagy and W. L. Hase, Chem. Phys. Lett. **54**, 73 (1978).
[12]R. A. Marcus, Faraday Discuss. Chem. Soc. **75**, 103 (1983); R. D. Taylor and P. Brumer, *ibid.* **75**, 117 (1983); E. J. Heller, *ibid.* **75**, 141 (1983).
[13]K. Rümpf and R. Mecke, Z. Phys. Chem. B **44**, 299 (1939); B. R. Henry and W. Siebrand, J. Chem. Phys. **49**, 5369 (1968).
[14]H. R. Dübal and M. Quack, Chem. Phys. Lett. **72**, 342 (1980).
[15]M. Quack, Faraday Discuss. Chem. Soc. **71**, 359 (1981).
[16]K. von Puttkamer, H. R. Dübal, and M. Quack, Faraday Discuss. Chem. Soc. **75**, 197, 263 (1983).
[17]J. E. Baggott, M.-C. Chuang, R. N. Zare, H. R. Dübal, and M. Quack,J. Chem. Phys. (to be published).
[18]S. Peyerimhoff, M. Lewerenz, and M. Quack, Chem. Phys. Lett. **109**, 563 (1984); H. R. Dübal, M. Lewerenz, and M. Quack, Faraday Discuss. Chem. Soc. **75**, 358 (1983).
[19]H. R. Dubal and M. Quack, Mol. Phys. (in press).
[20]G. Graner, R. Anttila, and J. Kauppinen, Mol. Phys. **38**, 103 (1979).
[21]S. Sofue, K. Kawaguichi, E. Hirota, and T. Fujiyama, Bull. Chem. Soc. Jpn. **54**, 897, 3546 (1981).
[22]G. Graner and G. Guelachvili, J. Mol. Spectrosc. (in press).
[23]H. R. Dübal and M. Quack, Chem. Phys. Lett. **80**, 439 (1981); M. Takami, H. R. Dübal, and M. Quack (in preparation).
[24]H. J. Bernstein and G. Herzberg, J. Chem. Phys. **16**, 30 (1948).
[25]A. Ruoff, H. Bürger, and S. Biedermann, Spectrochim. Acta Part A **27**, 1359 (1971); R. A. Ashby, J. Mol. Spectrosc. **28**, 265 (1968).
[26]R. W. Kirk and P. M. Wilt, J. Mol. Spectrosc. **58**, 102 (1975); N. J. Fyke, P. Lockett, J. K. Thompson, and P. M. Wilt, J. Mol. Spectrosc. **58**, 87 (1975); H. F. Chambers, R. W. Kirk, J. K. Thompson, M. J. Warner, and P. M. Wilt, *ibid.* **58**, 76 (1975); P. Lockett and P. M. Wilt, J. Chem. Phys. **60**, 3203 (1974).
[27]C. E. Blom and A. Müller, J. Mol. Spectrosc. **70**, 449 (1978).
[28]S. Saeki, M. Mizuno, and S. Kondo, Spectrochim. Acta Part A **32**, 403 (1974); S. Kondo and S. Saeki, J. Chem. Phys. **74**, 6603 (1981).
[29]T. E. Sullivan and L. Frenkel, J. Mol. Spectrosc. **39**, 185 (1971).
[30]W. L. Meerts and I. Ozier, J. Chem. Phys. **75**, 596 (1981).
[31]C. C. Costain, J. Mol. Spectrosc. **9**, 317 (1962); S. N. Gosh, R. Trambarulo, and W. Gordy, J. Chem. Phys. **20**, 605 (1952); H. D. Rix, *ibid.* **21**, 1077 (1953).
[32]Y. Kawashima and A. P. Cox, J. Mol. Spectrosc. **61**, 435 (1976); **72**, 423 (1978).
[33]J. P. Toennies (private communication).
[34]E. Fermi, Z. Phys. **71**, 250 (1931).
[35]U. White, J. Opt. Soc. Am. **32**, 285 (1942).
[36]A. R. H. Cole, *Tables of Wavenumber* (Pergamon, Oxford, 1977).
[37]G. Guelachvili, Opt. Commun. **8**, 171 (1973).
[38]C. Camy-Peyret, J. M. Flaud, and J. P. Maillard, J. Phys. Lett. **41**, 23 (1980); J. M. Flaud, C. Camy-Peyret, K. N. Rao, D-W. Chen and Y-S. Hoh, J. Mol. Spectrosc. **75**, 339 (1979).
[39]G. Pierre, J. C. Hilico, C. de Bergh, and J. P. Maillard, J. Mol. Spectrosc. **82**, 379 (1980).
[40]S. Califano, *Vibrational States* (Wiley, New York, 1976).
[41]P. Barchewitz, *Spectroscopie Infrarouge* (Gauthiers-Villars, Paris, 1961), Vol. 1.
[42]G. Amat, H. H. Nielsen, and C. Tarrago, *Rotation, Vibration of Polyatomic Molecules* (Dekker, New York, 1971).
[43]H. H. Nielsen, Phys. Rev. **60**, 794 (1941); Rev. Mod. Phys. **23**, 90 (1951).
[44]G. Amat and M. Goldsmith, J. Chem. Phys. **23**, 1171 (1955).
[45]E. L. Sibert III, J. T. Hynes, and W. P. Reinhardt, J. Phys. Chem. **87**, 2032 (1983).
[46]H. R. Dübal and M. Quack, Chem. Phys. Lett. **90**, 370 (1982); (to be published).
[47]J. H. Wilkinson and C. Reinsch, *Handbook for Automatic Computation Vol. 2, Linear Algebra* (Springer, Berlin, 1971).
[48]D. W. Marquardt, J. Soc. Ind. Appl. Math. **11**, 431 (1963).
[49]D. R. J. Boyd and H. C. Longuet-Higgins, Proc. R. Soc. London. Ser. A **213**, 55 (1952).
[50]I. Rossi, M. N. van Tanh, and C. Häusler, Can. J. Chem. **47**, 3319 (1969); T. A. Wiggins, E. R. Shull, and D. H. Rank, J. Chem. Phys. **21**, 1368 (1953).
[51]M. Quack, Adv. Chem. Phys. **50**, 395 (1982).
[52]M. Quack, Nuovo Cimento **38**, 358 (1981).
[53]J. S. Wong, R. A. Mac Phail, C. B. Moore, and H. L. Strauss, J. Chem. Phys. **86**, 1478 (1982).
[54]J. W. Perry, D. J. Moll, A. H. Zewail, and A. Kuppermann (preprint 1984); A. H. Zewail (private communication).
[55]O. Vierling and R. Mecke, Z. Phys. **99**, 204 (1936); H. L. Fang and R. L. Swofford, J. Chem. Phys. **72**, 6382 (1980).
[56]I. Abram, A. de Martino, and R. Frey, J. Chem. Phys. **76**, 5727 (1982).
[57]E. K. Plyler and E. D. Tidwell in Proceedings of the International Meeting of Molecular Spectroscopy, Bologna (1959), Vol. 3, p. 1336 (1962).